International Journal of Minerals, Metallurgy and Materials
Volume 23, Number 5, May 2016, Page 520
DOI: 10.1007/s12613-016-1263-7

Phosphate enrichment mechanism in $CaO–SiO_2–FeO–Fe_2O_3–P_2O_5$ steelmaking slags with lower binary basicity

Jin-yan Li[1)], *Mei Zhang*[1)], *Min Guo*[1)], *and Xue-min Yang*[2)]

1) State Key Laboratory of Advanced Metallurgy, School of Metallurgical and Ecological Engineering, University of Science and Technology Beijing, Beijing 100083, China

2) Key Laboratory of Green Process and Engineering, Institute of Process Engineering, Chinese Academy of Sciences, Beijing 100190, China

(Received: 2 June 2015; revised: 13 September 2015; accepted: 14 September 2015)

Abstract: The addition of silica to steelmaking slags to decrease the binary basicity can promote phosphate enrichment in quenched slag samples. In this study, we experimentally investigated phosphate enrichment behavior in $CaO–SiO_2–FeO–Fe_2O_3–P_2O_5$ slags with a P_2O_5 content of 5.00% and the binary basicity B ranging from 1.0 to 2.0, where the (%Fe_tO)/(%CaO) mass percentage ratio was maintained at 0.955. The experimental results are explained by the defined enrichment degree $R_{C_2S–C_3P}$ of solid solution $2CaO·SiO_2–3CaO·P_2O_5$ ($C_2S–C_3P$), where $R_{C_2S–C_3P}$ is a component of the developed ion and molecule coexistence theory (IMCT)–N_i model for calculating the mass action concentrations N_i of structural units in the slags on the basis of the IMCT. The asymmetrically inverse V-shaped relation between phosphate enrichment and binary basicity B was observed to be correlated in the slags under applied two-stage cooling conditions. The maximum content of P_2O_5 in the $C_2S–C_3P$ solid solution reached approximately 30.0% when the binary basicity B was controlled at 1.3.

Keywords: phosphates enrichment; mechanisms; steelmaking; slags; basicity

1. Introduction

High dephosphorization ability and a reasonable melting point are the basic and indispensable properties of traditional steelmaking slags. However, the enriched phosphate in steelmaking slags can adversely affect the recyclability in traditional metallurgical processes because of the limited refining ability. To dispose and reutilize accumulated steelmaking slags in an environmentally friendly manner, various techniques such as floatation [1], carbon reduction [2], and silicon reduction [3] for extracting phosphate from traditional steelmaking slags have been developed; however, none of these approaches has achieved the objective of simultaneously recycling the slags and reusing phosphate.

The principle of selective enrichment and phase separation [4−6], which has been applied to dispose slags with minimal boron [4], vanadium [5], and titanium [6] contents, can also be applied to extract phosphate from steelmaking slags. The selective enrichment and phase separation of phosphate in steelmaking slags [7] involve cooling molten slags with an optimized chemical composition under reasonable cooling conditions to promote the growth of phosphate-enriched grains. These grains can be obtained through phase separation based on differences between the physicochemical properties of the phosphate-enriched grains and the slags, such as differences in their density and magnetic field intensity.

Many researchers have investigated the enrichment behavior of phosphate in various slags [8−13]. In addition, we have previously elucidated the enrichment mechanism of phosphate in $CaO–SiO_2–FeO–Fe_2O_3–P_2O_5$ steelmaking slags with the binary basicity B ranging from 2.0 to 3.5 using X-ray powder diffraction (XRD), scanning electron microscopy (SEM), and energy-dispersive X-ray spectroscopy (EDS) [7]. These methods were used to observe the crystal structures of the components of quenched slag samples in this study. Meanwhile, the defined mass action concentration N_i based on the ion and molecule coexistence theory

Corresponding author: Min Guo E-mail: guomin@ustb.edu.cn

(IMCT) [7,14−17] was calculated to represent the reaction ability of structural units or ion couples in the slags. Moreover, we used the enrichment possibility N_{ci-cj} and enrichment degree R_{ci-cj} of phosphate to explain the experimental results [7] and deduced that the enrichment mechanism of phosphate in the slags involves the P_2O_5 component, which can easily bond with CaO to form tricalcium phosphate $3CaO·P_2O_5$ (C_3P). C_3P subsequently reacts with the produced dicalcium silicate, $2CaO·SiO_2$ (C_2S), to generate solid solution $C_2S–C_3P$ [18−19] under fixed cooling conditions. The maximum value of 84.4% for the defined enrichment degree $R_{C_2S-C_3P}$ of solid solution $C_2S–C_3P$ corresponds to a binary basicity B of 2.5 for the slags and (%Fe_tO)/(%CaO) mass percentage ratio of 0.955. However, the mass percentage of P_2O_5 in the phosphate-enriched phase obtained from the slags with a binary basicity B of 2.5 is approximately 16% [7], which is still lower than that of P_2O_5 obtained by Wang *et al*. [20−21] from modified steelmaking slags with a binary basicity B of 1.3. Wang *et al*. [20−21] further reported that decreasing the binary basicity B of steelmaking slags can effectively deplete the quantity of C_2S generated in the slags, thereby improving phosphate enrichment.

In the present study, we used methods similar to those reported in our previous study [7] to improve phosphate enrichment in traditional steelmaking slags by investigating the enrichment mechanism of phosphate in $CaO–SiO_2–FeO–Fe_2O_3–P_2O_5$ steelmaking slags in which the binary basicity B has been lowered by the addition of silica as a diluent. The optimized (%Fe_tO)/(%CaO) mass percentage ratio of 0.955 in the slags determined in our previous study [7] was also used in this study. The effects of binary basicity B in the range of 1.0–2.0 and P_2O_5 content in the range of 5.00%–10.00% on phosphate enrichment in the slags under the condition of (%Fe_tO)/(%CaO) = 0.955 were probed through experiments. Similarly, by combining the experimental and calculation results, we elucidated the phosphate enrichment mechanism in $CaO–SiO_2–FeO–Fe_2O_3–P_2O_5$ slags with the binary basicity B ranging from 1.0 to 2.0.

2. Description of IMCT–N_i thermodynamic model for $CaO–SiO_2–FeO–Fe_2O_3–P_2O_5$ slags based on IMCT

The defined mass action concentrations N_i of structural units or ion couples in slags, which are based on the IMCT [7,14−17] for metallurgical slags, can be used to reliably represent the reaction abilities of components, similar to traditionally applied activities $a_{R,i}$ of components relative to pure liquid or solid matter as the standard state in classical metallurgical physicochemistry. The reaction abilities of not only the components but also the formed species in the slags can be calculated using the developed IMCT–N_i thermodynamic model. The developed IMCT–N_i thermodynamic model for calculating the N_i of structural units or ion couples in $CaO–SiO_2–FeO–Fe_2O_3–P_2O_5$ slags based on the IMCT [7,14−17] has been reported in detail elsewhere [7]. For the benefit of the reader, the IMCT–N_i model developed for $CaO–SiO_2–FeO–Fe_2O_3–P_2O_5$ slags is briefly described here.

2.1. Structural units in $CaO–SiO_2–FeO–Fe_2O_3–P_2O_5$ slags

On the basis of the IMCT [7,14−17], the applied $CaO–SiO_2–FeO–Fe_2O_3–P_2O_5$ slag system is composed of Ca^{2+}, Fe^{2+}, and O^{2-} as three simple ions; SiO_2, Fe_2O_3, and P_2O_5 as three simple molecules; and $3CaO·SiO_2$ (C_3S), $2CaO·SiO_2$ (C_2S), $CaO·SiO_2$ (CS), etc. as 11 complex molecules according to the related binary and ternary phase diagrams [19,22] of $CaO–SiO_2$, $CaO–P_2O_5$, $CaO–FeO–SiO_2$, $CaO–FeO–P_2O_5$, etc. at elevated temperatures, as summarized in Table 1. This table is the same as that reported previously [7]. Notably, ($Ca^{2+} + O^{2-}$) and ($Fe^{2+} + O^{2-}$) should be treated as ion couples according to the IMCT [7,14−17].

According to the IMCT [7,14−17], the total equilibrium mole number Σn_i of all 16 structural units in 100 g slags can be expressed as

$$\Sigma n_i = 2n_1 + 2n_2 + n_3 + n_4 + n_5 + n_{c1} + n_{c2} + \cdots + n_{c11}, \quad \text{mol} \tag{1}$$

The defined [7,14−17] N_i of the structural unit i or ion couple ($Me^{2+} + O^{2-}$) can be described by

$$N_i = \frac{n_i}{\Sigma n_i}, \quad N_{MeO} = N_{Me^{2+},MeO} + N_{O^{2-},MeO} = \frac{n_{Me^{2+},MeO} + n_{O^{2-},MeO}}{\Sigma n_i} = \frac{2n_{MeO}}{\Sigma n_i} \tag{2}$$

All defined [7,14–17] equilibrium mole numbers n_i and mass action concentrations N_i of the formed structural units or ion couples in $CaO–SiO_2–FeO–Fe_2O_3–P_2O_5$ slags [7] are also listed in Table 1. Certainly, the mass action concentrations N_{ci} of all 11 complex molecules can be expressed by $K_{ci}^{\ominus}$, N_1 (N_{CaO}), N_2 (N_{SiO_2}), N_3 (N_{FeO}), N_4 ($N_{Fe_2O_3}$), and N_5 ($N_{P_2O_5}$) on the basis of the mass action law through $K_{ci}^{\ominus} = N_{ci} \Big/ \left(N_{Me1O}^{x} N_{Me2O}^{y}\right)$ by taking xMe1O·yMe2O as an example of complex or associated molecule ci.

2.2. Establishment of IMCT–N_i model for $CaO–SiO_2–FeO–Fe_2O_3–P_2O_5$ slags

The mass conservation equations of five components in

Table 1. Expressions of structural units as ion couples, simple or complex molecules, their mole number n_i, and mass action concentrations N_i in 100 g $CaO–SiO_2–FeO–Fe_2O_3–P_2O_5$ slags based on the IMCT

Item	Structural units as ion couples or molecules	No. of structural units or ion couples	Mole number n_i of structural units or ion couples / mol	Mass action concentration N_i of structural units or ion couples
Simple cations and anions (3)	$Ca^{2+}+O^{2-}$	1	$n_1=n_{Ca^{2+},CaO}=n_{O^{2-},CaO}=n_{CaO}$	$N_1=\frac{2n_1}{\Sigma n_i}=N_{CaO}$
	$Fe^{2+}+O^{2-}$	3	$n_3=n_{Fe^{2+},FeO}=n_{O^{2-},FeO}=n_{FeO}$	$N_3=\frac{2n_3}{\Sigma n_i}=N_{FeO}$
Simple molecules (3)	SiO_2	2	$n_2=n_{SiO_2}$	$N_2=\frac{n_2}{\Sigma n_i}=N_{SiO_2}$
	Fe_2O_3	4	$n_4=n_{Fe_2O_3}$	$N_4=\frac{n_4}{\Sigma n_i}=N_{Fe_2O_3}$
	P_2O_5	5	$n_5=n_{P_2O_5}$	$N_5=\frac{n_5}{\Sigma n_i}=N_{P_2O_5}$
Complex molecules (11)	$3CaO·SiO_2$	c1	$n_{c1}=n_{3CaO·SiO_2}$	$N_{c1}=\frac{n_{c1}}{\Sigma n_i}=N_{3CaO·SiO_2}$
	$2CaO·SiO_2$	c2	$n_{c2}=n_{2CaO·SiO_2}$	$N_{c2}=\frac{n_{c2}}{\Sigma n_i}=N_{2CaO·SiO_2}$
	$CaO·SiO_2$	c3	$n_{c3}=n_{CaO·SiO_2}$	$N_{c3}=\frac{n_{c3}}{\Sigma n_i}=N_{CaO·SiO_2}$
	$2FeO·SiO_2$	c4	$n_{c4}=n_{2FeO·SiO_2}$	$N_{c4}=\frac{n_{c4}}{\Sigma n_i}=N_{2FeO·SiO_2}$
	$2CaO·P_2O_5$	c5	$n_{c5}=n_{2CaO·P_2O_5}$	$N_{c5}=\frac{n_{c5}}{\Sigma n_i}=N_{2CaO·P_2O_5}$
	$3CaO·P_2O_5$	c6	$n_{c6}=n_{3CaO·P_2O_5}$	$N_{c6}=\frac{n_{c6}}{\Sigma n_i}=N_{3CaO·P_2O_5}$
	$4CaO·P_2O_5$	c7	$n_{c7}=n_{4CaO·P_2O_5}$	$N_{c7}=\frac{n_{c7}}{\Sigma n_i}=N_{4CaO·P_2O_5}$
	$3FeO·P_2O_5$	c8	$n_{c8}=n_{3FeO·P_2O_5}$	$N_{c8}=\frac{n_{c8}}{\Sigma n_i}=N_{3FeO·P_2O_5}$
	$4FeO·P_2O_5$	c9	$n_{c9}=n_{3FeO·P_2O_5}$	$N_{c9}=\frac{n_{c9}}{\Sigma n_i}=N_{4FeO·P_2O_5}$
	$2CaO·Fe_2O_3$	c10	$n_{c10}=n_{2CaO·Fe_2O_3}$	$N_{c10}=\frac{n_{c10}}{\Sigma n_i}=N_{2CaO·Fe_2O_3}$
	$FeO·Fe_2O_3$	c11	$n_{c11}=n_{FeO·Fe_2O_3}$	$N_{c11}=\frac{n_{c11}}{\Sigma n_i}=N_{FeO·Fe_2O_3}$

100 g slags can be established from the defined [7,14–17] n_i and N_i for all structural units (Table 1) and from Σn_i in Eq. (1) as

$$b_1=\left(\frac{1}{2}N_1+3N_{c1}+2N_{c2}+N_{c3}+2N_{c5}+3N_{c6}+4N_{c7}+2N_{c10}\right)\Sigma n_i=\left(\frac{1}{2}N_1+3K_{c1}^{\ominus}\ N_1^3N_2+2K_{c2}^{\ominus}\ N_1^2N_2+K_{c3}^{\ominus}\ N_1N_2+2K_{c5}^{\ominus}\ N_1^2N_5+3K_{c6}^{\ominus}\ N_1^3N_5+4K_{c7}^{\ominus}\ N_1^4N_5+2K_{c10}^{\ominus}N_1^2N_4\right)\Sigma n_i=n_{CaO}^0,\ \text{mol} \quad (3a)$$

$$b_2=(N_2+N_{c1}+N_{c2}+N_{c3}+N_{c4})\Sigma n_i=(N_2+K_{c1}^{\ominus}\ N_1^3N_2+K_{c2}^{\ominus}\ N_1^2N_2+K_{c3}^{\ominus}\ N_1N_2+K_{c4}^{\ominus}\ N_2N_3^2)\Sigma n_i=n_{SiO_2}^0,\ \text{mol} \quad (3b)$$

$$b_3=\left(\frac{1}{2}N_3+2N_{c4}+3N_{c8}+4N_{c9}+N_{c11}\right)\Sigma n_i=\left(\frac{1}{2}N_3+2K_{c4}^{\ominus}\ N_2N_3^2+3K_{c8}^{\ominus}\ N_3^3N_5+4K_{c9}^{\ominus}\ N_3^4N_5+K_{c11}^{\ominus}N_3N_4\right)\Sigma n_i=n_{FeO}^0,\ \text{mol} \quad (3c)$$

$$b_4=(N_4+N_{c10}+N_{c11})\Sigma n_i=(N_4+K_{c10}^{\ominus}N_1^2N_4+K_{c11}^{\ominus}N_3N_4)\Sigma n_i=n_{Fe_2O_3}^0,\ \text{mol} \quad (3d)$$

$$b_5 = (N_5 + N_{c5} + N_{c6} + N_{c7} + N_{c8} + N_{c9})\Sigma n_i = (N_5 + K_{c5}^{\ominus}\ N_1^2 N_5 + K_{c6}^{\ominus}\ N_1^3 N_5 + K_{c7}^{\ominus}\ N_1^4 N_5 + K_{c8}^{\ominus}\ N_3^3 N_5 + K_{c9}^{\ominus}\ N_3^4 N_5)\Sigma n_i = n_{P_2O_5}^0, \quad \text{mol} \tag{3e}$$

According to the principle that the sum of the equilibrium mole fractions of all structural units in a fixed amount of slags under equilibrium conditions is equal to unity, we obtain

$$N_1 + N_2 + N_3 + N_4 + N_5 + N_{c1} + N_{c2} + N_{c3} + N_{c4} + N_{c5} + N_{c6} + N_{c7} + N_{c8} + N_{c9} + N_{c10} + N_{c11} = N_1 + N_2 + N_3 + N_4 + N_5 + K_{c1}^{\ominus}\ N_1^3 N_2 + K_{c2}^{\ominus}\ N_1^2 N_2 + K_{c3}^{\ominus}\ N_1 N_2 + K_{c4}^{\ominus}\ N_2 N_3^2 + K_{c5}^{\ominus}\ N_1^2 N_5 + K_{c6}^{\ominus}\ N_1^3 N_5 + K_{c7}^{\ominus}\ N_1^4 N_5 + K_{c8}^{\ominus}\ N_3^3 N_5 + K_{c9}^{\ominus}\ N_3^4 N_5 + K_{c10}^{\ominus} N_1^2 N_4 + K_{c11}^{\ominus} N_3 N_4 = 1.0 \tag{4}$$

Eqs. (3)–(4) are composed of the governing equations of the developed IMCT–N_i model for calculating the mass action concentrations N_i of structural units or ion couples in $CaO–SiO_2–FeO–Fe_2O_3–P_2O_5$ slags. Obviously, the developed IMCT–N_i model includes six unknown parameters, i.e., N_1 (N_{CaO}), N_2 (N_{SiO_2}), N_3 (N_{FeO}), N_4 ($N_{Fe_2O_3}$), N_5 ($N_{P_2O_5}$), and Σn_i, with six independent equations. The unique solution of N_i, Σn_i, and n_i can be obtained by solving the algebraic equation group of Eqs. (3)–(4) by combining these equations with the definition of N_i in Eq. (2).

The developed IMCT–N_i model was applied to calculate the N_i of structural units or ion couples in slags with the binary basicity B ranging from 1.0 to 2.0 at an interval of 0.05 and with the P_2O_5 mass percentage and (%Fe$_t$O)/(%CaO) mass percentage ratio maintained at 5.00% and 0.955, respectively.

3. Experimental

3.1. Preparation of synthetic slags

The investigated $CaO–SiO_2–FeO–Fe_2O_3–P_2O_5$ slag system was synthesized from the prepared ferrous oxide (FeO) powder samples and reagent-grade CaO, SiO_2, Fe_2O_3, and P_2O_5 powders. In accordance with the method suggested by Pahlevani *et al*. [23], the FeO powder samples were prepared by mixing pure powders of iron and reagent-grade Fe_2O_3 in a pure iron crucible and heating the mixture under an argon atmosphere at 1673 K for 60 min. The prepared FeO powder samples and the reagent-grade powders of CaO, SiO_2, Fe_2O_3, and P_2O_5 were mixed in a platinum crucible with an inner diameter in 30.0 mm and a height in 50.0 mm. The platinum crucible with the mixed slag samples was placed in an Al_2O_3 crucible to allow easy removal of the samples from the furnace during experiments.

A vertical-tube-type furnace with $MoSi_2$ rods as heating elements was used in conjunction with a programmed heating/cooling routine. The temperature precision of the heating furnace was approximately ± 3 K. High-purity argon (99.999vol%) was controlled at a flow rate of 0.4 L/min as a carrier gas to avoid the re-oxidation of the prepared FeO during heating and cooling of the slag samples in test-run experiments.

Eight test-run experiments were performed to investigate the influence of binary basicity B in the range of 1.0–2.0 on the phosphate enrichment behavior in the quenched slag samples. The chemical compositions of the eight slag samples are summarized in the left columns of Table 2. The binary basicity values B of the slags in test-run experiment Nos. 1–7 were individually designed as 1.0, 1.2, 1.3, 1.4, 1.5, 1.7, and 2.0 under the conditions of a P_2O_5 mass percentage of 5.00% and (%Fe$_t$O)/(%CaO) mass percentage ratio of 0.955; these conditions were determined in a previous study [7] to promote phosphate enrichment. In addition, to probe the influence of the initial P_2O_5 content on phosphate enrichment in the slags, we designed test-run experiment No. 8, in which the P_2O_5 mass percentage was fixed at 10.00% under conditions of a binary basicity B of 1.3 and (%Fe$_t$O)/(%CaO) ratio of 0.955.

3.2. Experimental procedures

The heating program differed from the cooling program. The heating schedule is described as follows: (1) the platinum crucible containing the mixed slag sample was placed into the furnace at ambient temperature; (2) high-purity Ar gas at a flow rate of 0.4 L/min was charged into the reaction tube for at least 30 min before the furnace power was switched on; (3) the sample was heated under an Ar atmosphere from ambient temperature to a fixed temperature of 1773 K at a rate of 2.0–5.0 K/min using a proportional–integral–derivative (PID) controller; and (4) the temperature was maintained 1773 K for 30 min under an Ar atmosphere to completely melt and fully synthesize the slags. By contrast, the cooling schedule consisted of the following steps: (1) the furnace temperature was decreased from 1773 to 1573 K at a rate of 2.0 K/min; (2) the temperature was maintained at 30 min at 1573 K to promote growth of phosphate-enriched grains; (3) the temperature was further decreased from 1573 to 1373 K at 2.0 K/min as a secondary slow-cooling stage to further promote condensation; and (4) the temperature was maintained at 1373 K for another 30 min as a secondary isothermal stage to ensure complete condensation.

Table 2. Chemical compositions of eight synthesized slag samples with a (%Fe_tO)/(%CaO) mass percentage ratio of 0.955 and corresponding EDS analysis results

Test No.	Position	Zones	Chemical composition of slags / wt%					Binary basicity, B	EDS analysis results / wt%				Average of P_2O_5 / wt%
			CaO	SiO_2	FeO	Fe_2O_3	P_2O_5		CaO	SiO_2	Fe_3O_4	P_2O_5	
1	1	white	31.56	31.56	14.35	17.53	5.00	1.0	0.20	0.69	98.53	0.58	—
	2	gray							33.16	40.56	19.84	6.44	6.44
2	3	white	33.41	27.84	15.19	18.56	5.00	1.2	0.21	0.02	99.77	tr.	—
	4	white							0.16	0.02	99.82	tr.	—
	5	gray							42.28	26.68	26.21	4.82	—
	6	gray							41.64	27.21	26.31	4.84	—
	7	dark							42.78	26.71	18.40	12.11	12.11
3	8	white	34.18	26.29	15.54	18.99	5.00	1.3	0.22	0.81	98.49	0.48	—
	9	white							0.29	0.65	98.67	0.39	—
	10	gray							36.31	39.55	18.99	5.14	—
	11	gray							36.75	38.68	18.33	6.24	—
	12	dark							52.13	15.79	0.93	31.15	31.09
	13	dark							51.08	16.81	1.09	31.02	
4	14	white	34.87	24.91	15.85	19.37	5.00	1.4	0.28	0.02	99.70	0.00	—
	15	white							0.22	0.02	99.76	0.00	—
	16	gray							44.07	30.15	23.50	2.27	—
	17	gray							44.57	30.30	22.72	2.41	—
	18	dark							61.69	17.61	5.78	14.92	16.62
	19	dark							62.19	16.45	4.23	17.13	
	20	dark							62.35	15.87	3.99	17.79	
5	21	white	35.49	23.66	16.13	19.72	5.00	1.5	0.45	0.83	98.72	0.00	—
	22	white							0.40	1.04	98.17	0.39	—
	23	gray							36.35	39.20	21.12	3.33	—
	24	gray							35.61	39.32	20.92	4.15	—
	25	dark							51.38	29.07	5.06	14.49	13.82
	26	dark							51.23	30.19	5.42	13.16	
6	27	white	36.56	21.51	16.62	20.31	5.00	1.7	1.02	0.80	98.18	0.00	—
	28	white							1.29	tr.	98.24	0.47	—
	29	gray							36.55	41.02	19.44	2.99	—
	30	gray							36.62	42.69	18.50	2.18	—
	31	dark							51.56	33.14	6.04	9.27	13.72
	32	dark							53.23	25.38	3.21	18.18	
7	33	white	37.85	18.92	17.20	21.03	5.00	2.0	1.05	0.66	98.30	0.00	—
	34	gray							29.59	34.66	34.49	1.26	—
	35	dark							53.96	26.93	6.11	13.00	13.00
8	36	white	32.38	24.91	14.72	17.99	10.00	1.3	0.35	0.09	99.56	tr.	—
	37	gray							36.77	33.33	26.09	3.81	—
	38	dark							55.67	7.00	7.26	30.07	30.04
	39	dark							55.47	7.35	7.17	30.01	

Note: "tr." indicates that the concentration of a component was lower than the minimum detection limit of the EDS analyzer.

Afterwards, the platinum crucible containing the slag sample was immediately removed from the furnace and rapidly quenched in a water pool. The obtained slag samples were dried in an oven at 403 K for at least 4 h. The dried slag samples were used as raw materials for the subsequent detection of mineralogical phases, as described in Section 3.3.

Importantly, the $(\%FeO)/(\%Fe_2O_3)$ mass percentage ratio in the slag samples was kept almost constant during melting and condensation because high-purity Ar gas was flowing into the furnace tube during each test run. To avoid any change of valence of the iron in Fe_tO amphoteric oxides, the Ar gas with 99.999% purity was rigorously purified by a gas purification train for approximately 1 h before the heating procedure was started. With regard to the gas purification train, the moisture was removed by passing the Ar gas through columns containing silica gel and dry anhydrous magnesium perchlorate $Mg(ClO_4)_2$; the CO_2 content was then lowered by passing the Ar gas through a column of Ascarite, and oxygen impurities in the Ar gas were subsequently oxidized using two furnaces in series containing copper turnings maintained at 973 K and magnesium turnings maintained at 773 K.

3.3. Detection of mineralogical phases in slag samples

The methods used to characterize the mineralogical phases in the slag samples in this study were the same as those used in our previous study [7]. The XRD experiments were performed on a powder X-ray diffractometer (Rigaku Dmax-2500) equipped with a Cu-K_α radiation source to identify the crystal structure of the quenched slag samples. For observation of the micromorphology of the quenched slag samples, the samples were mounted in epoxy resin, ground with SiC sandpapers, polished, and coated with carbon for SEM (JSM–6480) analysis. The EDS was subsequently used to construct elemental mapping images and to further identify the chemical composition of the microstructures formed in the quenched slag samples.

4. Results and discussion

4.1. Characterization of crystal phases in slags

The EDS results for eight slag samples are summarized in the right-hand side of Table 2. The influence of binary basicity *B*, which ranged from 1.0 to 2.0, on the mass percentage of P_2O_5 in the phosphate-enriched phase, as determined by EDS analysis of the quenched slags, is shown in Fig. 1. Obviously, the greatest mass percentage of P_2O_5 in a phosphate-enriched phase was 31.09%, as observed for the test run No. 3.

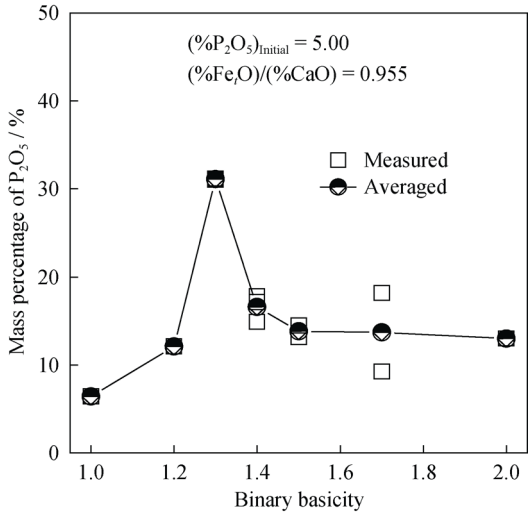

Fig. 1. Relation between binary basicity *B* in a range of 1.0–2.0 and P_2O_5 mass percentage in the phosphate-enriched phase, as determined by EDS analysis, in quenched slag samples. The $(\%P_2O_5)$ and $(\%Fe_tO)/(\%CaO)$ mass percentage ratio in samples were maintained at 5.00 and 0.955, respectively.

The three slag samples labeled as No. 1, No. 3, and No. 7 in Table 2 were selected as representative slag samples for detection of the crystal structure in the slags via XRD analysis. The XRD patterns of the aforementioned three slag samples are displayed in Fig. 2. In the case of slag sample No. 1 (Fig. 2(a)), whose binary basicity *B* was 1.0, the main mineralogical phases are Fe_3O_4 and compound CS; the phosphate-enriched phase was not detected. In the case of slag sample No. 3 (Fig. 2(b)), whose binary basicity *B* was 1.3, the main mineralogical phases are Fe_3O_4 and $Ca_3Fe_2(SiO_4)_3$, and the phosphate-enriched phase is detected as a $C_2S–C_3P$ solid solution. In the case of slag sample No. 7 (Fig. 2(c)), whose binary basicity *B* was 2.0, the main mineralogical phases are Fe_3O_4, compound C_2S, and solid solution $C_2S–C_3P$.

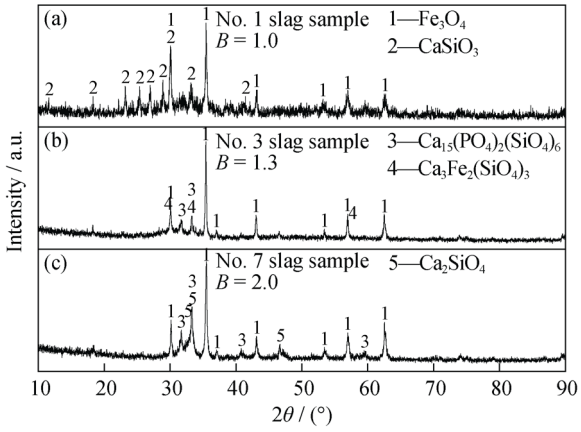

Fig. 2. X-ray diffraction patterns of slag samples obtained from test runs No. 1 (a), No. 3 (b), and No. 7 (c).

SEM and EDS analyses were used to identify the chemical compositions of the microstructures formed in the quenched slag samples. The SEM image of slag sample No. 3 is shown in Fig. 3(a). The corresponding EDS mapping images of elements Ca, Fe, P, Si, and O in slag sample No. 3 are also illustrated in Figs. 3(b)–(f), respectively. Three zones — white, gray, and dark zones — are clearly evident in slag sample No. 3 in Fig. 3(a). On the basis of the results in Fig. 3(c), Fig. 3(f), and Fig. 3(a), the white zone in Fig. 3(a) is composed primarily of Fe and O; i.e., it is an iron-oxide- enriched phase. Similarly, a comparison of results in Fig. 3(b), Fig. 3(c), and Fig. 3(e) with those in Fig. 3(a) reveals that the gray zone in Fig. 3(a) consists of Ca, Fe, and Si; i.e., this zone is the matrix phase. Moreover, combining the results in Fig. 3(b), Fig. 3(d), and Fig. 3(e) with those in Fig. 3(a) reveals that the dark zone in Fig. 3(a) is composed primarily of Ca, Si, and P; i.e., it is the phosphate-enriched phase.

We deduced that the elements Fe and O detected in the white zone could exist as Fe_3O_4; while the Ca, Fe, and Si detected in the gray zone as the matrix phase could exist as calcium silicate (CS–C_2S) and kirschsteinite ($CaO{\cdot}SiO_2{\cdot}FeO$),

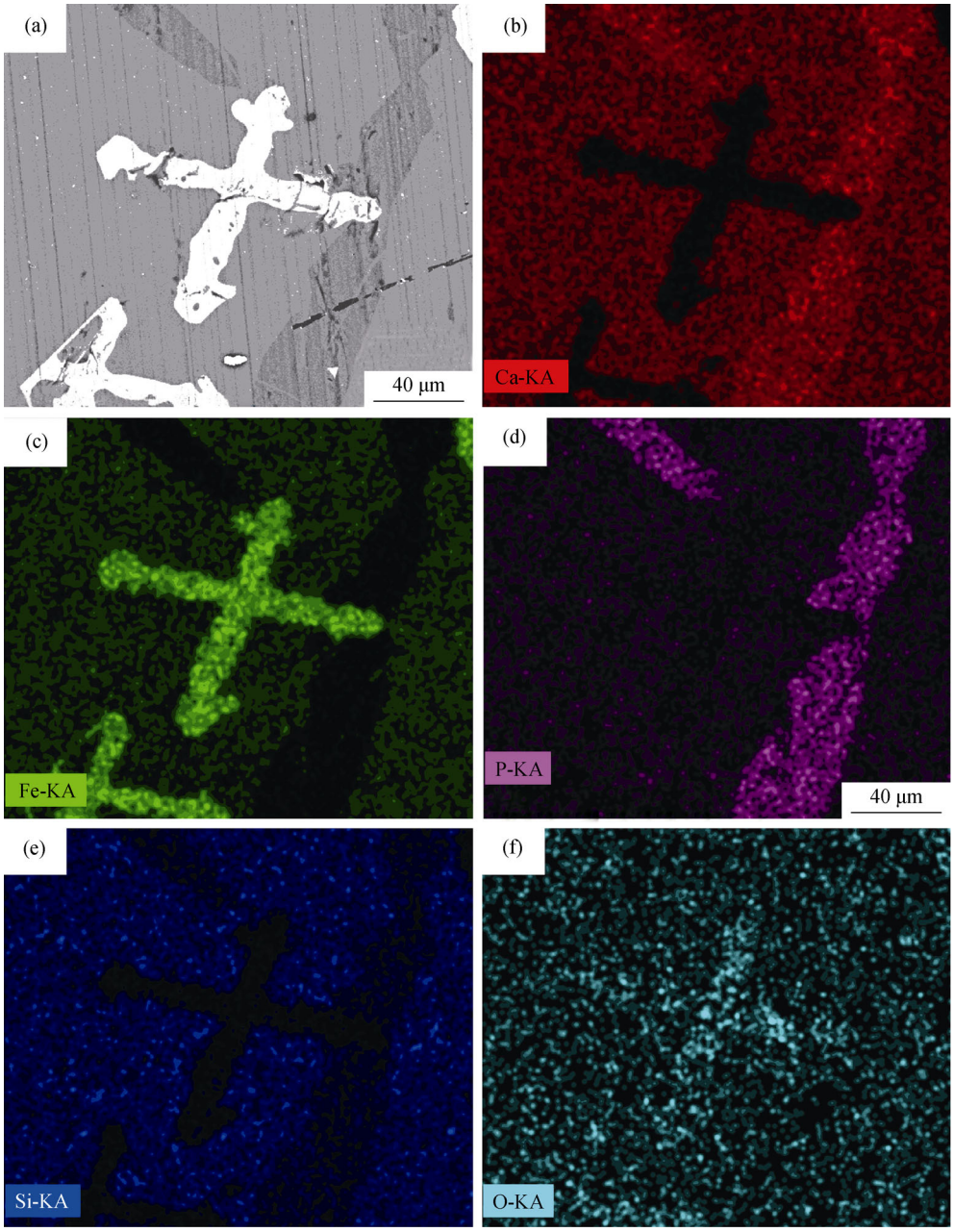

Fig. 3. SEM images of slag sample No. 3 (a) and corresponding EDS mapping images of Ca (b), Fe (c), P (d), Si (e), and O (f) in quenched slag samples with binary basicity *B* as 1.3 and (%P_2O_5) as 5.00.

and the Ca, Si, and P detected in the dark zone could exist as solid solution C_2S–C_3P.

The SEM images of the slag samples from test runs No. 1–No. 8 are displayed in Fig. 4. In the case of slag sample No. 1, whose binary basicity *B* was 1.0, we combined the SEM image in Fig. 4(a) with the corresponding EDS results for point 1 and point 2 in Table 2 and deduced that iron oxides dominate the white zone assigned as point 1 in Fig. 4(a); by contrast, we deduced that a phosphate phase is dispersed in the gray zone as the matrix phase assigned as point 2 in Fig. 4(a). No phosphate-enriched phase, i.e., no dark zone, was observed in Fig. 4(a).

In the case of slag sample No. 2, whose binary basicity *B* was 1.2, we combined the SEM image in Fig. 4(b) with the corresponding EDS results from point 3 to point 7 in Table 2 and deduced that iron oxides dominate the white zones represented by point 3 and point 4 in Fig. 4(b); we also deduced that a large amount of the matrix phase was generated as the gray zone represented by point 5 and point 6. In addition, a small amount of solid solution C_2S–C_3P was also formed as the dark zone indicated by point 7. The presence of this solid solution was deduced by comparing the results in Fig. 4(a) with those in Fig. 4(b); the results of this comparison indicate that increasing the binary basicity *B* from 1.0 to 1.2 can promote the formation of this dark phase. However, the amount of dark phase formed is not sufficient to be precipitated as dark stripes. The corresponding EDS results from point 5 to point 7 in Table 2 further indicate that the determined mass percentage of P_2O_5 at point 5 and point 6 (gray phase) is lower than that at point 7 (dark phase); this result implies that parts of phosphate can be condensed from the gray matrix phase into the dark, stripe-shaped phase.

In the case of slag sample No. 3, whose binary basicity *B* was 1.3, we combined the SEM image in Fig. 4(c) with the corresponding EDS results from point 12 to point 13 in Table 2 and deduced that the dark phase can clearly be produced as a columnar shape. According to the mass percentage of P_2O_5 at point 12 and point 13 (dark phase) determined by the EDS and reported in Table 2, phosphate can be well enriched in the dark phase, where the mass percentage of P_2O_5 in the phosphate-enriched phase can reach approximately 31.00%. Notably, the results obtained for the points in white and gray phases will not be discussed in the following text.

In the case of slag sample No. 4, whose binary basicity *B* was 1.4, the combination of the SEM image in Fig. 4(d) with the corresponding EDS results from point 18 to point 20 in Table 2 reveals that the dark phase, i.e., the phosphate-enriched phase, exhibits a granular shape. A comparison of the SEM image of slag sample No. 3 in Fig. 4(c) with that of slag sample No. 4 in Fig. 4(d) reveals that an increase in the binary basicity *B* from 1.3 to 1.4 can lead to an obvious variation of the shape of the dark phase from column to granule. Meanwhile, a comparison of the mass percentage of P_2O_5 determined by EDS for slag sample No. 3 slag with that for slag sample No. 4 in Table 2 reveals that an increase in the binary basicity *B* from 1.3 to 1.4 can also result in a significantly decrease in the P_2O_5 mass percentage from 31.09% to 16.62%; i.e., the extent of phosphate enrichment is substantially diminished. This phenomenon can be interpreted as an increase in the binary basicity leading to in an increase in the quantity of C_2S generated. Thus, we deduced that the number of crystal nuclei formed during instantaneous nucleation in Fig. 4(d) is greater than that in Fig. 4(c). The generated C_3P phase (dark phase) with unchangeable quantity can widely disperse in smaller-sized shapes, as shown in Fig. 4(d). Thus, an increase in the quantity of C_2S formed can lead to an increase of the dark-phase area. Consequently, the mass percentage of P_2O_5 in the dark phase should, compared with that in Fig. 4(c), decrease under the condition of a binary basicity *B* of 1.4.

From the viewpoint of promoting phosphate enrichment, the optimal binary basicity *B* of the slags is approximately 1.30. Thus, the results from slag sample No. 3 in Fig. 4(c) and in Table 2 were selected as criteria for comparison in this section.

As demonstrated in the case of slag samples No. 5 (Fig. 4(e)) and No. 6 (Fig. 4(f)), whose binary basicity *B* values were 1.5 and 1.7, respectively, increasing the binary basicity *B* from 1.3 in the case of slag sample No. 3 (Fig. 4(c)) to 1.5 or 1.7 in the cases of these slag samples clearly does not lead to substantial variation in the shapes of white and dark phases. Comparing the mass percentage of P_2O_5 determined by EDS for slag samples No. 5 and No. 6 slag with that obtained for No. 4 slag sample (Table 2) reveals that an increase in the binary basicity *B* to 1.5 and 1.7 can deteriorate the phosphate-enrichment behavior. Interestingly, the boundaries between the gray phase and dark phase for slag sample No. 6 (Fig. 4(f)), whose binary basicity *B* was 1.7, were not as clear as those observed in slag sample No. 5 (Fig. 4(e)), whose binary basicity *B* was 1.5. Thus, the formed calcium silicate phase in the matrix phase (gray phase) and the generated phosphate-enriched phase (dark phase) exhibit greater affinity for transferring CS to C_2S at a binary basicity *B* of 1.7.

As demonstrated in the case of slag sample No. 7 (Fig. 4(g)), whose binary basicity *B* was 2.0, a further increase in

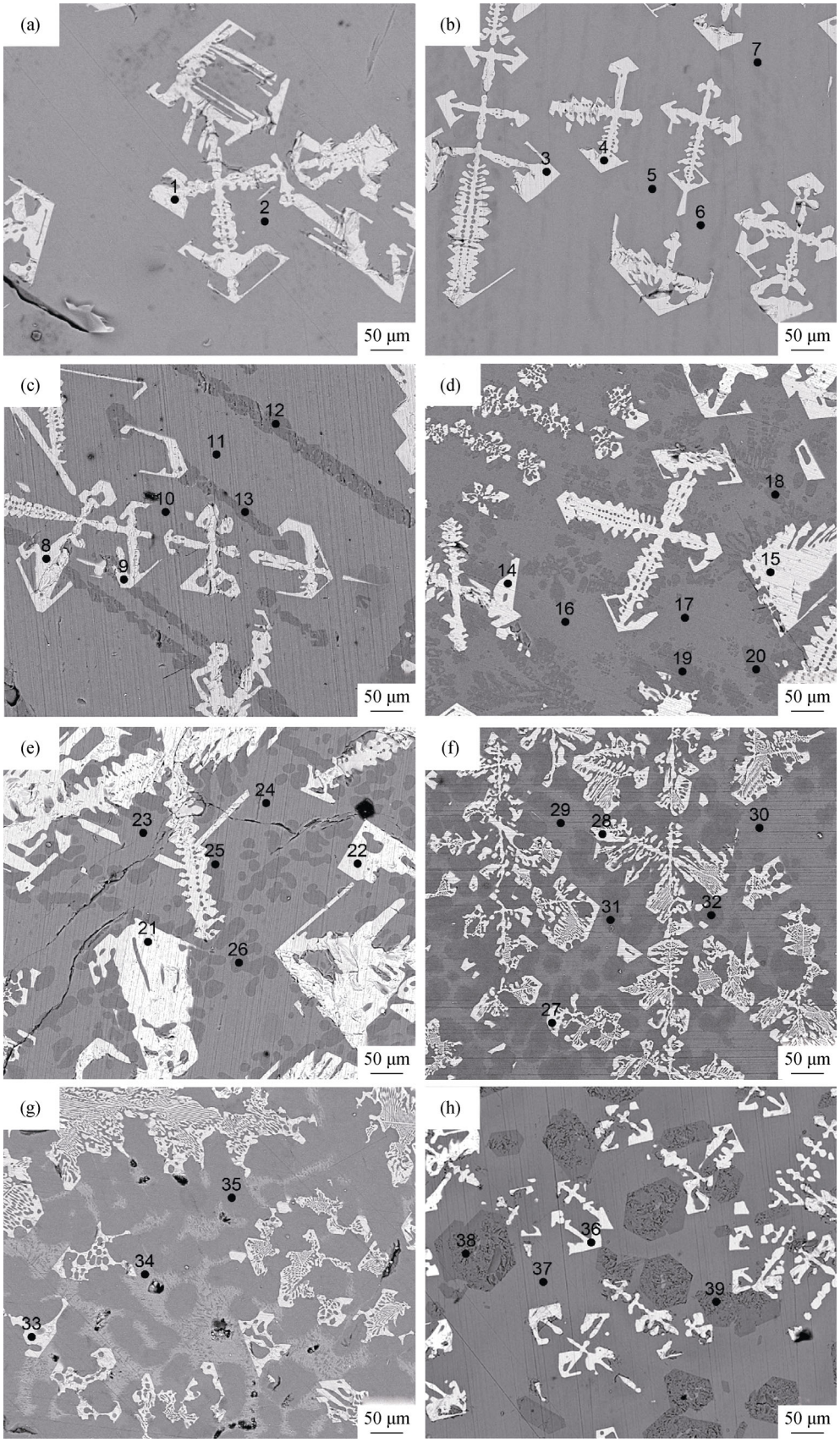

Fig. 4. SEM images of quenched slag samples obtained from test runs No. 1 to No. 8 (a–h, respectively). The (%Fe_tO)/(%CaO) mass percentage ratio was maintained at 0.955.

the binary basicity B from 1.7 to 2.0 did not lead to substantial changes in the shapes of white and gray phases compared to the shapes observed in slag sample No. 6 (Fig. 4(f)) with a binary basicity B of 1.7. However, an increase of the binary basicity B from 1.7 to 2.0 did cause an increase of the dark-phase area in Fig. 4(g). We deduced that increasing the binary basicity B from 1.7 to 2.0 does not obviously affect the phosphate enrichment results.

Fig. 4(h) shows the SEM image of slag sample No. 8, whose binary basicity B was 1.3, prepared under the condition of a P_2O_5 mass percentage of 10.00%. Comparing the SEM results for slag sample No. 3 in Fig. 4(c) with those for slag sample No. 8 in Fig. 4(h) leads to the conclusion that increasing the initial mass percentage of P_2O_5 in the slag sample from 5.00% to 10.00% obviously affects the SEM results; specifically, the area of the dark phase is obviously enlarged. However, comparing the summarized results of the mass percentage of P_2O_5 determined by EDS for slag sample No. 3 with those for slag sample No. 8 in Table 2 reveals that increasing the initial mass percentage of P_2O_5 in the slag sample from 5.00% to 10.00% does not lead to detectable variation of the determined mass percentage of P_2O_5 in the phosphate-enriched phase. Thus, increasing the initial mass percentage of P_2O_5 from 5.00% to 10.00% can only facilitate formation of the phosphate-enriched phase, not increase the mass percentage of P_2O_5 in the enriched phase. This result implies that the maximum value of phosphate enrichment of approximately 30.00% is not affected by varying the initial mass percentage of P_2O_5 in the slag samples under conditions of a binary basicity B of 1.3 and a $(\%Fe_tO)/(\%CaO)$ mass percentage ratio of 0.955.

4.2. Discussion

4.2.1. Effect of binary basicity on the mass action concentrations N_i of six structural units

According to the developed IMCT–N_i model described in Section 2, three complex molecules of calcium silicates — $3CaO·SiO_2$ (C_3S), $2CaO·SiO_2$ (C_2S), and $CaO·SiO_2$ (CS) — can be formed in $CaO–SiO_2–FeO–Fe_2O_3–P_2O_5$ slags; in addition, three main complex molecules that contain P_2O_5 — $2CaO·P_2O_5$ (C_2P), $3CaO·P_2O_5$ (C_3P), and $4CaO·P_2O_5$ (C_4P) — can also be generated in the slags. Fig. 5(a) shows the relation between the binary basicity B in the range of 1.0–2.0 and the calculated N_{ci} of the aforementioned three calcium silicates as C_3S, C_2S, and CS for slags at a temperature of 1773 K and in which the mass percentage of P_2O_5 and the $(\%Fe_tO)/(\%CaO)$ mass percentage ratio are maintained at 5.00% and 0.955, respectively. Similarly, the relation between the binary basicity in the range of 1.0–2.0 and the calculated N_{cj} of the three main complex molecules containing P_2O_5 (C_2P, C_3P, and C_4P) in the slags under the same conditions is illustrated in Fig. 5(b). The results in Fig. 5(a) indicate that the calculated value of N_{C_3S} is much smaller than the calculated values of N_{C_2S} and N_{CS}, consistent with the reported $CaO–SiO_2$ phase diagram [19]. Thus, the contribution of C_3S to the formed calcium silicates can be disregarded. Increasing the binary basicity B from 1.0 to 2.0 can result in an increasing trend of the calculated N_{C_2S} value but a decreasing trend of the N_{CS} value. Obviously, the calculated N_{CS} and N_{C_2S} values exhibit competing

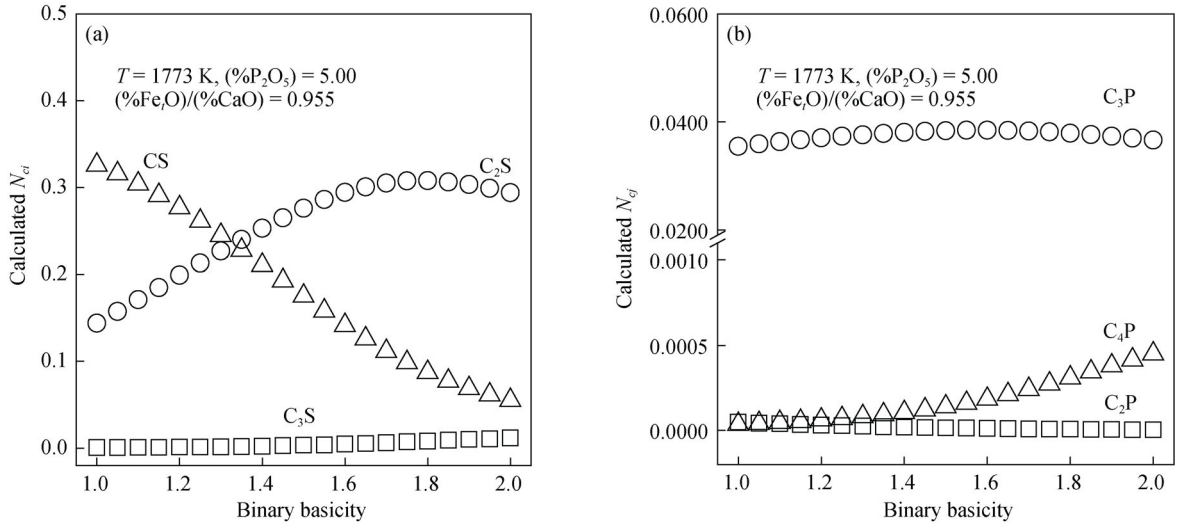

Fig. 5. Relation of binary basicity in a range of 1.0–2.0 at interval of 0.05 and calculated mass action concentrations N_{ci} of three calcium silicates as C_3S, C_2S, or CS (a) or calculated mass action concentrations N_{cj} of three P_2O_5-containing structural units as C_2P, C_3P, or C_4P (b) for $CaO–SiO_2–FeO–Fe_2O_3–P_2O_5$ slags at a temperature of 1773 K under the conditions of $(\%P_2O_5)$ = 5.00 and $(\%Fe_tO)/(\%CaO)$ = 0.955.

behaviors for the slags with the binary basicity B between 1.0 and 2.0.

According to Fig. 5(b), the calculated N_{C_3P} is substantially greater than the calculated N_{C_2P} and N_{C_4P}. The calculated N_{C_3P} exhibits an asymmetrically parabolic trend as the binary basicity B is increased from 1.0 to 2.0. The maximum value of the calculated N_{C_3P} corresponds to a binary basicity B of 1.7. The influence of binary basicity B in the range of 1.0–2.0 on the calculated N_{C_2P} is opposite its influence on N_{C_4P}. Thus, increasing the binary basicity B from 1.0 to 2.0 can result in a decreasing tendency of N_{C_2P} but an increasing tendency of N_{C_4P}.

4.2.2. Phosphate enrichment phenomenon at binary basicity less than 1.3

To explain the tendency of the phosphate enrichment in the quenched slag samples to decrease when the binary basicity B is less than 1.3, we apply the enrichment possibility N_{ci-cj} of phosphate as well as the enrichment degree $R_{ci\text{-}cj}$ of phosphate in slags defined in our previous study [7]. Because the calculated N_{C_2P} and N_{C_4P} values are much smaller than the calculated N_{C_3P}, as shown in Fig. 5(b), the contribution of C_3P to phosphate enrichment is substantially greater than the contributions of C_2P and C_4P. Thus, the contributions of both C_2P and C_4P to the enrichment possibility N_{ci-cj} of phosphate and to the enrichment degree $R_{ci\text{-}cj}$ of phosphate in the slags can be disregarded.

Under this circumstance, the enrichment possibility N_{ci-C_3P}, which is defined as the product of the calculated N_{ci} for complex molecule ci containing calcium silicates and the calculated N_{C_3P}, can be expressed by

$$N_{C_2S-C_3P} = N_{C_2S}N_{C_3P},\quad N_{CS-C_3P} = N_{CS}N_{C_3P},$$
$$N_{C_3S-C_3P} = N_{C_3S}N_{C_3P} \tag{5}$$

The summation of the enrichment possibility N_{ci-C_3P} for all three of the aforementioned structural units can be expressed as

$$\sum\left(N_{ci-C_3P}\frac{M_{P_2O_5}}{M_{ci-C_3P}}\right) = N_{C_2S}N_{C_3P}\frac{M_{P_2O_5}}{M_{C_2S-C_3P}} + N_{CS}N_{C_3P}\frac{M_{P_2O_5}}{M_{CS-C_3P}} + N_{C_3S}N_{C_3P}\frac{M_{P_2O_5}}{M_{C_3S-C_3P}} \tag{6}$$

Thus, the ratio of the defined [7] enrichment possibility N_{ci-C_3P} to the summation of the enrichment possibility for all three of the aforementioned structural units, i.e., $\sum\left(N_{ci-C_3P}\frac{M_{P_2O_5}}{M_{ci-C_3P}}\right)$, is defined as enrichment degree $R_{ci\text{-}C_3P}$. The defined enrichment degree $R_{C_2S\text{-}C_3P}$ of solid solution C_2S–C_3P can be calculated by

$$R_{C_2S\text{-}C_3P} = \frac{N_{C_2S}N_{C_3P}\frac{M_{P_2O_5}}{M_{C_2S-C_3P}}}{N_{C_2S}N_{C_3P}\frac{M_{P_2O_5}}{M_{C_2S-C_3P}} + N_{CS}N_{C_3P}\frac{M_{P_2O_5}}{M_{CS-C_3P}} + N_{C_3S}N_{C_3P}\frac{M_{P_2O_5}}{M_{C_3S-C_3P}}} = \frac{N_{C_2S}\frac{M_{P_2O_5}}{M_{C_2S-C_3P}}}{N_{C_2S}\frac{M_{P_2O_5}}{M_{C_2S-C_3P}} + N_{CS}\frac{M_{P_2O_5}}{M_{CS-C_3P}} + N_{C_3S}\frac{M_{P_2O_5}}{M_{C_3S-C_3P}}} \tag{7}$$

Fig. 6 shows the relation of binary basicity B in the range of 1.0–1.3 to the enrichment degree $R_{C_2S-C_3P}$ of solid solution C_2S–C_3P or to the mass percentage of P_2O_5 in the phosphate-enriched phase determined by EDS analysis of the quenched slags, in which the initial mass percentage of P_2O_5 was 5.00%. Although the enrichment degree $R_{C_2S-C_3P}$ of solid solution C_2S–C_3P based on the IMCT [7,14–17] is greater than the determined mass percentage of P_2O_5 in the phosphate-enriched phase in the quenched slag samples with the binary basicity B less than 1.3, a similar increasing tendency of the enrichment degree $R_{C_2S-C_3P}$ of solid solution C_2S–C_3P or the determined mass percentage of P_2O_5 in the phosphate-enriched phase is observed when the binary basicity B is less than 1.3. Thus, the enrichment degree $R_{C_2S-C_3P}$ of solid solution C_2S–C_3P calculated on the basis of the IMCT [7,14–17] can be used to predict the phosphate enrichment phenomenon in the quenched slag samples with the binary basicity B less than 1.3.

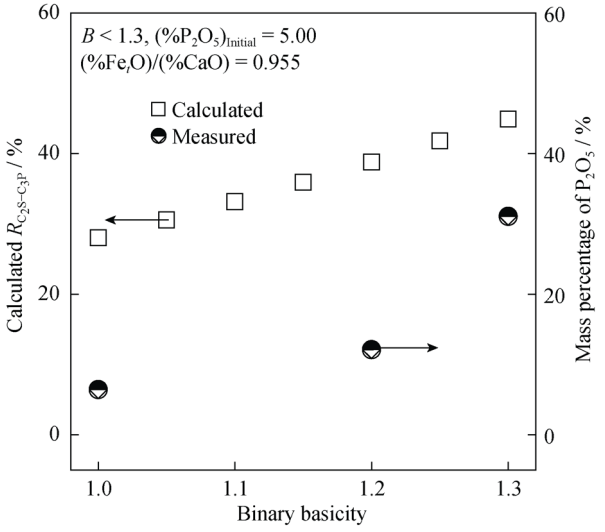

Fig. 6. Relation between binary basicity B in a range of 1.0–1.3 and calculated enrichment degree $R_{C_2S-C_3P}$ or determined mass percentage of P_2O_5 in the phosphate-enriched phase in quenched slag samples in which (%P_2O_5) is 5.00.

By combining the experimental results obtained from the SEM images in Fig. 4(a) or Fig. 4(b) with the calculation results in Fig. 5(a), we deduced that the produced C_2S, rather than CS, is the main precursor that bonds C_3P in the quenched slag samples with the binary basicity B less than 1.3. However, greater N_{CS} in the slags with the binary basicity B less than 1.3 does not promote phosphate enrichment in the quenched slag samples. Certainly, the enrichment degree $R_{C_2S-C_3P}$ of solid solution C_2S–C_3P cannot explain the decreasing trend of the mass percentage of P_2O_5 in the phosphate-enriched phase for the quenched slag samples with the binary basicity B greater than 1.3.

Notably, the enrichment degree $R_{C_2S-C_3P}$ of solid solution C_2S–C_3P and the mass percentage of P_2O_5 in the phosphate-enriched phase are both distinct parameters and are related to each other provided that the entire slag system is correctly defined.

4.2.3. Phosphate enrichment phenomenon at binary basicity greater than 1.3

According to the definition of N_i in Eq. (2), the equilibrium mole number n_i can be calculated as $n_i = N_i \Sigma n_i$. Thus, the mole fraction of C_3P in solid solution C_2S–C_3P can be calculated by

$$x_{C_3P} = n_{C_3P} \Big/ \left(n_{C_2S} + n_{C_3P}\right) = N_{C_3P} \Sigma n_i \Big/ \left(N_{C_2S} + N_{C_3P}\right) \Sigma n_i = N_{C_3P} \Big/ \left(N_{C_2S} + N_{C_3P}\right) \quad (8)$$

The mass percentage of C_3P in solid solution C_2S–C_3P can be determined as

$$(\%C_3P) = 100 \times \frac{n_{C_3P} \times M_{C_3P}}{n_{C_2S} \times M_{C_2S} + n_{C_3P} \times M_{C_3P}} = 100 \times \frac{N_{C_3P} \times M_{C_3P} \times \Sigma n_i}{\left(N_{C_2S} \times M_{C_2S} + N_{C_3P} \times M_{C_3P}\right) \times \Sigma n_i} \quad (9)$$

The mass percentage of P_2O_5 in solid solution C_2S–C_3P can be predicted by

$$(\%P_2O_5) = (\%C_3P) \times \frac{M_{P_2O_5}}{M_{C_3P}} = 100 \times \frac{N_{C_3P} \times M_{P_2O_5}}{N_{C_2S} \times M_{C_2S} + N_{C_3P} \times M_{C_3P}} \quad (10)$$

Fig. 7(a) shows the relation between the binary basicity B in the range of 1.3–2.0 and the calculated mole fraction x_{C_3P} of C_3P in solid solution C_2S–C_3P or the mass action concentration ratio $N_{C_3P} \Big/ \left(N_{C_2S} + N_{C_3P}\right)$ for the slags at a temperature of 1773 K and with the mass percentage of P_2O_5 fixed at 5.00%. Meanwhile, Fig. 7(b) shows the relation of the binary basicity B in the range of 1.3–2.0 to the mass percentage of P_2O_5 in the phosphate-enriched phase determined by EDS analysis or to the mass percentage of P_2O_5 in solid solution C_2S–C_3P calculated on the basis of Eq. (10) for the slags. As shown in Fig. 7(a), an increase of the binary basicity B from 1.3 to 2.0 can cause an obvious decreasing trend of the mass action concentration ratio $N_{C_3P} \Big/ \left(N_{C_2S} + N_{C_3P}\right)$ in the slags. Meanwhile, the mass percentage of P_2O_5 in solid solution C_2S–C_3P, as calculated by Eq. (10), also tends to increase as the binary basicity B is increased from 1.3 to 2.0. Moreover, the mass percentage of P_2O_5 in solid solution C_2S–C_3P, as calculated by Eq. (10), is in good agreement with the mass percentage of P_2O_5 in the phosphate-enriched phase determined by EDS analysis. The greater amount of C_2S can decrease the phosphate enrichment

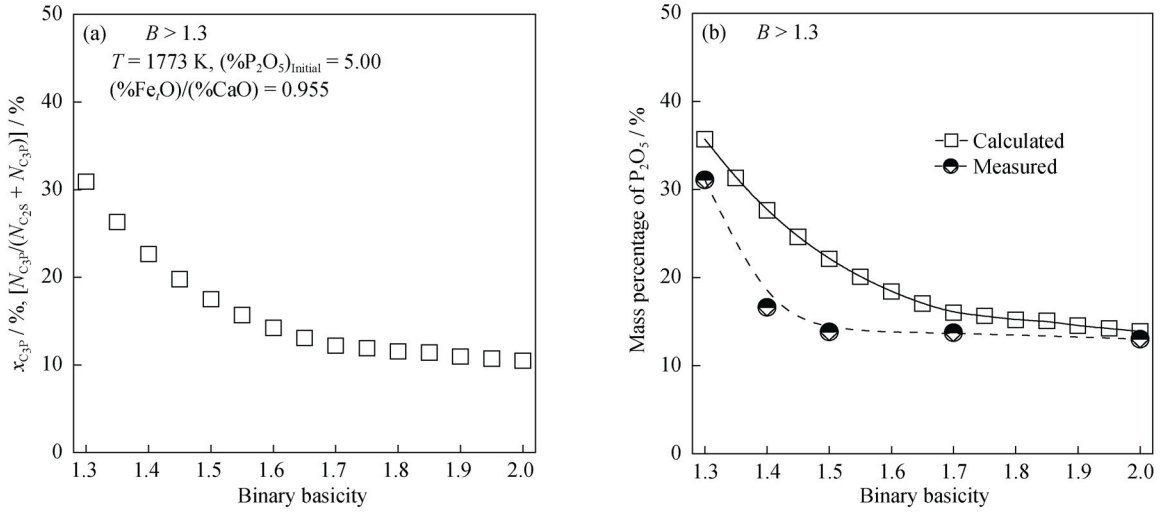

Fig. 7. Relation between binary basicity B in a range of 1.3–2.0 and calculated mole fraction x_{C_3P} of C_3P in solid solution C_2S–C_3P or calculated mass action concentration ratio $N_{C_3P} \Big/ \left(N_{C_2S} + N_{C_3P}\right)$ (a) and mass percentage of P_2O_5 in the phosphate-enriched phase determined by EDS analysis or calculated mass percentage of P_2O_5 in solid solution C_2S–C_3P (b) in quenched slag samples in which (%P_2O_5) is 5.00.

in the quenched slag samples when the binary basicity B is greater than 1.3.

Combining the results in Fig. 6 with those in Fig. 7 leads to the reasonable deduction: (1) most phosphate will exist as C_3P in the slags at elevated temperatures; (2) the formed C_3P can be easily bonded with C_2S to produce solid solution C_2S–C_3P in the quenched slag samples; (3) maintaining the binary basicity B at 1.3 can result in the maximum phosphate enrichment for the slags with a P_2O_5 mass percentage of 5.00% and a (%Fe_tO)/(%CaO) mass percentage ratio of 0.955; (4) the phosphate enrichment in the quenched slag samples with the binary basicity B less than 1.3 can be predicted on the basis of their C_2S content; (5) the phosphate enrichment in the quenched slag samples with the binary basicity B greater than 1.3 can be predicted on the basis of the C_3P content in the solid solution C_2S–C_3P and on the basis of a greater amount of C_2S diminishing the phosphate enrichment in the quenched slag samples.

Thus, a binary basicity B of 1.3, a P_2O_5 content of 5.00%, and a (%Fe_tO)/(%CaO) the mass percentage ratio of 0.955 are recommended to promote selective phosphate enrichment and phase separation of the investigated steelmaking slags.

5. Conclusions

Phosphate enrichment behavior has been experimentally investigated in CaO–SiO_2–FeO–Fe_2O_3–P_2O_5 slags with the binary basicity B ranging from 1.0 to 2.0 and with the mass percentage ratio (%Fe_tO)/(%CaO) maintained at 0.955. The experimental results have been explained by the defined enrichment degree R_{ci-C_3P} of solid solutions containing P_2O_5. This defined enrichment degree is a component of the developed IMCT–N_i model for calculating the mass action concentrations N_i of structural units in the slags. The main findings are summarized as follows.

(1) The asymmetrically inverse V-shaped relation between the binary basicity B in the range of 1.0–2.0 and the phosphate enrichment in the quenched slag samples can be correlated for slags under the applied two-stage cooling conditions. The maximum content of P_2O_5 in solid solution $2CaO{\cdot}SiO_2$–$3CaO{\cdot}P_2O_5$ (C_2S–C_3P) is approximately 30.0% and is obtained for slags with a binary basicity B of 1.3 and in which the mass percentage ratio (%Fe_tO)/(%CaO) was maintained at 0.955.

(2) The promotive effect of binary basicity B in the range of 1.0–1.3 on the phosphate enrichment in the quenched slag samples with a P_2O_5 content of 5.00% can be quantitatively explained by the defined enrichment degree $R_{C_2S-C_3P}$ of the solid solution C_2S–C_3P in the slags. The formed C_2S, rather than CS, in the slags with binary basicity B ranging from 1.0 to 1.3 can be bonded by C_3P to form the solid solution $2CaO{\cdot}SiO_2$–$3CaO{\cdot}P_2O_5$ (C_2S–C_3P) under fixed cooling conditions.

(3) The deteriorative effect of binary basicity B in the range of 1.3–2.0 on phosphate enrichment in the quenched slag samples with a P_2O_5 content of 5.00% can be quantitatively explained on the basis of the calculated C_3P content in the solid solution C_2S–C_3P. Although increasing the binary basicity B from 1.3 to 2.0 can improve the absolute amount of C_2S, the C_3P content in the solid solution C_2S–C_3P tends to decrease as the binary basicity B of the slags is increased within this range.

Acknowledgements

The work was financially supported by the National Basic Research Program of China (No. 2014CB643401) and by the National Natural Science Foundation of China (Nos. 51372019, 51174186, and 51072022).

References

[1] H. Ono, A. Inagaki, T. Masui, H. Narita, T. Mitsuo, S. Nosaka, and S. Gohda, Removal of phosphorus from LD converter slag by floating of dicalcium silicate during solidification, *Tetsu-to-Hagané*, 66(1980), No. 6, p. 1317.

[2] K. Morita, M.X. Guo, N. Oka, and N. Sano, Resurrection of the iron and phosphorus resource in steel-making slag, *J. Mater. Cycles Waste Manage.*, 4(2002), No. 2, p. 93.

[3] S. Takeuchi, N. Sano, and Y. Matsushita, Separate recovery of iron and phosphorus from BOF slags using Fe–Si alloys, *Tetsu-to-Hagané*, 66(1980), No. 14, p. 2050.

[4] Z.T. Sui and P.X. Zhang, Selective precipitating behavior of the boron components from the boron slag, *Acta Metall. Sin.*, 33(1997), No. 9, p. 943.

[5] X.R. Wu, L.S. Li, and Y.C. Dong, Influence of P_2O_5 on crystallization of V concentrating phase in V-bearing steelmaking slag, *ISIJ Int.*, 47(2007), No. 3, p. 402.

[6] L. Zhang, L.N. Zhang, M.Y. Wang, G.Q. Li, and Z.T. Sui, Dynamic oxidation of the Ti-bearing blast furnace slag, *ISIJ Int.*, 46(2006), No. 3, p. 458.

[7] J.Y. Li, M. Zhang, M. Guo, and X.M. Yang, Enrichment mechanism of phosphate in CaO–SiO_2–FeO–Fe_2O_3–P_2O_5 steelmaking slags, *Metall. Mater. Trans. B*, 45(2014), No. 5, p. 1666.

[8] W. Fix, H. Heymann, and R. Heinke, Subsolidus relations in the system $2CaO{\cdot}SiO_2$–$3CaO{\cdot}P_2O_5$, *J. Am. Ceram. Soc.*, 52(1969), No. 6, p. 346.

[9] K. Ito, M. Yanagisawa, and N. Sano, Phosphorus distribution between solid $2CaO{\cdot}SiO_2$ and molten CaO–SiO_2–FeO–Fe_2O_3

slags, *Tetsu-to-Hagané*, 68(1982), No. 2, p. 342.

[10] R. Inoue and H. Suito, Phosphorous Partition between $2CaO·SiO_2$ Particles and $CaO–SiO_2–Fe_tO$ slags, *ISIJ Int.*, 46(2006), No. 2, p. 174.

[11] H. Suito and R. Inoue, Behavior of phosphorous transfer from $CaO–Fe_tO–P_2O_5(–SiO_2)$ slag to CaO particles, *ISIJ Int.*, 46(2006), No. 2, p. 180.

[12] R. Inoue and H. Suito, Mechanism of dephosphorization with $CaO–SiO_2–Fe_tO$ slags containing mesoscopic scale $2CaO·SiO_2$ particles, *ISIJ Int.*, 46(2006), No. 2, p. 188.

[13] T. Hamano, S. Fukagai, and F. Tsukihashi, Reaction mechanism between solid CaO and $FeO_x–CaO–SiO_2–P_2O_5$ slag at 1573 K, *ISIJ Int.*, 46(2006), No. 4, p. 490.

[14] X.M. Yang, M. Zhang, J.L. Zhang, P.C. Li, J.Y. Li, and J. Zhang, Representation of oxidation ability for metallurgical slags based on the ion and molecule coexistence theory, *Steel Res. Int.*, 85(2014), No. 3, p. 347.

[15] X.M. Yang, J.P. Duan, C.B. Shi, M. Zhang, Y.L. Zhang, and J.C. Wang, A thermodynamic model of phosphorus distribution ratio between $CaO–SiO_2–MgO–FeO–Fe_2O_3–MnO–Al_2O_3–P_2O_5$ slags and molten steel during a top–bottom combined blown converter steelmaking process based on the ion and molecule coexistence theory, *Metall. Mater. Trans. B*, 42(2011), No. 4, p. 738.

[16] X.M. Yang, C.B. Shi, M. Zhang, J.P. Duan, and J. Zhang, A Thermodynamic model of phosphate capacity for $CaO–SiO_2–MgO–FeO–Fe_2O_3–MnO–Al_2O_3–P_2O_5$ slags equilibrated with molten steel during a top–bottom combined blown converter steelmaking process based on the ion and molecule coexistence theory, *Metall. Mater. Trans. B*, 42(2011), No. 5, p. 951.

[17] J. Zhang, *Computational Thermodynamics of Metallurgical Melts and Solutions*, Metallurgical Industry Press, Beijing, China, 2007.

[18] E.J. Drewes, M. Olette, Investigations of the effect of siliccon oxide and of the oxidation degree on the phase boundaries, in particular of the miscibility gap, in the system $CaO–P_2O_5–FeO–Fe_2O_3–SiO_2$ at 1600°C, *Arch. Eisenhuttenwes.*, 38(1967), No. 3, p. 163.

[19] Verein Deutscher Eisenhüttenleute, *Slag Atlas*, 2nd Ed, Woodhead Publishing Limited, Abington Hall, Abington, Cambridge, CB21 6AH, UK, 1995, p. 63, 138, 139.

[20] N. Wang, Z.G. Liang, M. Chen, and Z.S. Zou, Phosphorous enrichment in molten adjusted converter slag: Part I. Effect of adjusting technological conditions, *J. Iron Steel Res. Int.*, 18(2011), No. 11, p. 17.

[21] N. Wang, Z.G. Liang, M. Chen, and Z.S. Zou, Phosphorous enrichment in molten adjusted converter slag: Part II. Enrichment behavior of phosphorus in $CaO–SiO_2–FeO_x–P_2O_5$ molten slag, *J. Iron Steel Res. Int.*, 18(2011), No. 12, p. 22.

[22] J.X. Chen, *Handbook of Common Figures*, *Tables and Data for Steelmaking*, Metallurgical Industry Press, Beijing, 1984.

[23] F. Pahlevani, S. Kitamura, H. Shibata, and N. Maruoka, Distribution of P_2O_5 between solid solution of $2CaO·SiO_2–3CaO·P_2O_5$ and liquid phase, *ISIJ Int.*, 50(2010), No. 6, p. 822.